



ORIGINAL ARTICLE

Molecular modelling and optical properties of a novel fluorinated chalcone

J.M.F. Custodio^{a,*}, J.J.A. Guimarães-Neto^b, R. Awad^b, J.E. Queiroz^b,
G.M.V. Verde^b, M. Mottin^a, B.J. Neves^{a,c}, C.H. Andrade^a, G.L.B. Aquino^b,
C. Valverde^{b,d}, F.A.P. Osório^{a,e}, B. Baseia^a, H.B. Napolitano^{b,c}

^a Universidade Federal de Goiás, Goiânia, GO, Brazil

^b Universidade Estadual de Goiás, Anápolis, GO, Brazil

^c Centro Universitário de Anápolis, GO, Brazil

^d Universidade Paulista, Goiânia, GO, Brazil

^e Pontifícia Universidade Católica de Goiás, Goiânia, GO, Brazil

Received 13 August 2018; accepted 11 November 2018

Available online 17 November 2018

KEYWORDS

Molecular modeling;
NLO properties;
Fluorinated chalcone

Abstract Chalcones exhibit a broad spectrum of biological activities, mainly due to α,β -unsaturated ketone, and are precursors of the biosynthesis of flavonoids present in plants. These compounds have been shown to be useful in the biological approach, proven by the broad spectrum of biological activities reported, and also in the technological approach, considering their potential as nonlinear optic (NLO) material. In this context, this work aimed to examine the crystallization and characterization of fluorinated chalcone (E)-1-(4-fluorophenyl)-3-(4-isopropylphenyl)prop-2-en-1-one (DFC). A comprehensive structural study of DFC was carried out to understand the process of stabilizing the crystalline lattice through X-ray diffraction, infrared spectroscopy, and molecular modeling studies. Finally, the electrical properties of DFC were calculated by using the supermolecule method (SM). DFC molecules are connected by means of C—H...O and C—H...F intermolecular contacts, forming dimers which play an important role in the stabilization of crystal packing. Molecular modeling studies indicated that this compound could act as an anti-tuberculosis ligand because of its high binding affinity with the *M. tuberculosis* enoyl-acyl carrier protein, InhA. On the other hand, theoretical calculations were performed to evaluate the NLO properties of DFC and indicated that it showed good potential.

© 2018 Production and hosting by Elsevier B.V. on behalf of King Saud University. This is an open access article under the CC BY-NC-ND license (<http://creativecommons.org/licenses/by-nc-nd/4.0/>).

* Corresponding author.

E-mail address: jeanmfcustodio@gmail.com (J.M.F. Custodio).

Peer review under responsibility of King Saud University.



Production and hosting by Elsevier

1. Introduction

Chalcones, or 1,3-diphenyl-2-propen-1-one, are important open-chain flavonoids present in the plant kingdom and occur mainly as phenolic compounds colored yellow to orange. Chalcone exist as trans (E) or cis (Z) isomers with two aromatic

rings joined by an α,β -unsaturated ketone group ($-\text{C}(\text{O})\text{CH}=\text{CH}-$); the most stable and predominant stereoisomer is the E isomer (Gomes et al., 2017; Rosa et al., 2017). Furthermore, chalcone can be obtained from natural sources (Abu et al., 2013) and synthetic methods. There are several methods for the synthesis of chalcones, including the classical method of Claisen-Schmidt condensation (Murugesan et al., 2017; Joui et al., 2016), Wittig's reactions (Szczesna et al., 2017; Gharib et al., 2014) and the Friedel-Crafts acylation (Das et al., 2014; Calloway and Green, 1937).

In fact, chalcones are bioactive against virtually all eukaryotes and some prokaryotes, and their molecular targets are numerous (Díaz-Tielas et al., 2016). Considering these aspects, the synthesis and characterization of new chalcone analogues with enhanced properties are continuous fields in research (Díaz-Tielas et al., 2016). Chalcones exhibit a broad spectrum of biological activities, mainly due to α,β -unsaturated ketone and are precursors of the biosynthesis of flavonoids found in plants (Climent et al., 1995) which may act as a Michael acceptor, and also due to the substitution pattern in the aromatic rings, which interfere either positively or negatively in electron delocalization in the molecule. Therefore, the presence of a double bond in conjunction with the carbonyl group is responsible for the biological activities of chalcones (Gonçalves et al., 2014).

Chemically, its molecular skeleton is defined by portions of aromatic rings attached through a three-carbon bridge with a keto-carbonyl group and an α, β unsaturation (Climent et al., 1995). Biological activities include anticancer, anti-inflammatory, antibacterial, anti-tuberculosis, antidiabetic, anti-oxidant, antimicrobial, antiviral, antimalarial, anthelmintic, antiprotozoal, cytotoxic and insecticidal (Nowakowska, 2007; Matos et al., 2015), and neuroprotective effects, among others (Zhou, 2015; Mahapatra et al., 2015; Hameed et al., 2016; Ferreira et al., 2014; Wan et al., 2015). Based on these characteristics, the study of structural issues and the synthetic perspective is an extension and understanding of the applicability of the molecule.

In addition, chalcones also stand out for their efficiency in Second-Harmonic Generation (SHG) and present a remarkable third-order nonlinearity, since they crystallize in a non-symmetrical structure (Mahapatra et al., 2015; Krawczyk et al., 2016). Several papers discuss the nonlinear properties of chalcones (Vaz et al., 2016; Carvalho et al., 2017; Castro et al., 2017), which are related to the delocalization of π electrons in the molecule since they can be easily polarized.

Thus, the present paper focuses on the synthesis and crystallographic characterization of the chalcone (E)-1-(4-fluorophenyl)-3-(4-isopropylphenyl)prop-2-en-1-one (DFC) in terms of bond lengths and angles, molecular interactions and its supramolecular arrangement. Furthermore, the DFC bulk was analyzed to predict its potential biological activities as an anti-tuberculosis agent. The static and dynamic electrical properties of the DFC crystal were theoretically studied using the supermolecule method (SM) to simulate the crystalline environment polarization on a single DFC isolated molecule. Møller-Plesset Perturbation Theory (MP2) was employed to calculate the dipole moment and the linear polarizability and Density Functional Theory (DFT) at CAM-B3LYP level was used to obtain the second hyperpolarizability, both using the 6-311+G(d) basis set. We also present an estimate of the linear refractive index and the third-order susceptibility for the DFC

crystal and study the effect of a solvent medium on the electric parameters of a DFC isolated molecule.

2. Experimental and computational procedures

2.1. Synthesis and crystallization

The melting point was recorded in a MQAPF-301 apparatus and was uncorrected. The chromatogram and mass spectrum were recorded in a GCMS QP2010 Ultra (Shimadzu), equipped with CBP-5 capillary column (30 m \times 0.25 μm \times 0.25 mm), injection volume of 1.0 μL , Split and Helium as carrier gas (1.0 mL/min). The temperature of the injector was maintained at 280 $^{\circ}\text{C}$ and the detector at 310 $^{\circ}\text{C}$. The initial oven temperature was 100 $^{\circ}\text{C}$, maintained for 2 min, followed by a heating ramp to 300 $^{\circ}\text{C}$ at 30 $^{\circ}\text{C}/\text{min}$ and maintained for 10 min at 300 $^{\circ}\text{C}$. IR spectra were recorded in a FT-IR Frontier (PerkinElmer) spectrophotometer. ^1H and ^{13}C NMR spectra were performed on an aAvance III (Bruker) spectrometer, operating at 500 MHz (^1H) and 126 MHz (^{13}C), and their chemical shifts are recorded in δ (parts per million) units with respect to tetramethyl silane (TMS) as internal standard. All the reagents and solvents used were of analytical grade and were used as supplied. Progress of the reactions was monitored using TLC, performed on aluminum chromate sheets with silica gel 60, Alugram® Xtra Sil G, with indicator UV254 (Macherey-Nagel) and the spots were visualized by exposure to iodine vapors or UV camera.

Equimolar quantities (1 mmol) of 4-fluoroacetophenone and 4-isopropylbenzaldehyde were mixed and dissolved in a minimum amount (2 mL) of absolute alcohol. For this, powdered KOH was added slowly, and the mixture homogenized until precipitation, at room temperature. Completion of the reaction was identified by TLC. After completion of the reaction, the solid precipitate was filtered and dried. It was purified by recrystallization in hot absolute alcohol. The crystal growth was obtained in methanol under slow evaporation. Mol. formula: $\text{C}_{18}\text{H}_{17}\text{FO}$; 268.33 g/mol; white crystals; mp 72.8–74 $^{\circ}\text{C}$; yield 77%.

The structure of the synthesized compound was confirmed by analysis of FTIR spectrum, which the peak at 1650 cm^{-1} of carbonyl ($\text{C}=\text{O}$) and at 1601 cm^{-1} of double bonded to carbonyl ($-\text{C}=\text{C}-$). Other peaks were $\nu\text{C}-\text{H}$ sp³ at 2932 cm^{-1} ; $\nu\text{C}-\text{H}$ sp² at 3000 cm^{-1} ; $\nu\text{C}-\text{F}$ at 1245 cm^{-1} and $\nu\text{C}-\text{H}$ of propyl at 755 cm^{-1} . Mass spectrum (m/z): 268 ($\text{M}^+ + 1$); exact mass of molecular ion = 268.33. ^1H NMR (δ ppm): 8.07 (m, 2H), 7.83 (d, $J = 15.7$ Hz, 1H), 7.60 (m, 2H), 7.48 (d, $J = 15.7$ Hz, 1H), 7.31 (m, 2H), 7.20 (m, 2H), 2.97 (hept, $J = 6.9$ Hz, 1H), 1.31 (s, 3H), 1.29 (s, 3H); and ^{13}C NMR (δ ppm): 189.00; 167.57; 164.45; 152.19; 145.19; 134.76; 132.46; 131.08; 131.00; 128.63; 127.13; 126.26; 120.73; 115.78; 115.61; 34.15; 23.78; 23.71.

2.2. Crystallographic characterization

The X-ray diffraction data of DFC were obtained by a Bruker APEX II CCD diffractometer with graphite-mono chromate $\text{MoK}\alpha$ radiation ($\lambda = 0.71073$ Å), where the DFC crystals were maintained at room temperature (298 K). The structure was solved by direct methods and refined by full-matrix least-squares on F^2 using SHELXL2014 (Sheldrick, 2015).

Molecular representations, tables and pictures were obtained through the programs Ortep (Farrugia, 2012), Mercury (Macrae et al., 2006) and Crystal Explorer (Spackman and Jayatilaka, 2009) using WinGXplatform (Farrugia, 2012). The possible interactions of hydrogen were checked by PARST (Nardelli, 1995). The crystallographic data were deposited at the Cambridge Crystallographic Data Center (CCDC) (Battle et al., 2010; Allen, 2002) under the number 1844553. Copies of the data can be obtained, free of charge, via www.ccdc.cam.ac.uk.

2.3. Target prediction

The 3D structure of DFC in Mol2 format was submitted to PharmMapper web server, for prediction of potential biological activities by fitting small molecules into structure-based pharmacophore models (Liu et al., 2010; Wang et al., 2017). We performed the prediction, keeping most parameters as default, except the maximum conformations set up to 300, and the number of reserved matched targets set up to 300.

2.4. Ligand and protein preparation

The 3D structure of the DFC was prepared in Marvin Sketch v.6.3.1 software (ChemAxon, Budapest, Hungary, <http://www.chemaxon.com>) at pH = 7.4. Subsequently, up to 2000 conformers were generated using OMEGA v.3.0.0.1, (Hawkins et al., 2010; OMEGA, 2018), and the AM1-BCC charges (Jakalian et al., 2002) were added using QUACPAC v. 1.7.0.2 (QUACPAC, n.d.). In parallel, the protonation states of 3D structures of the predicted protein targets were predicted by H++ server (Anandakrishnan et al., 2012; Gordon et al., 2005) at neutral pH (7.4 ± 1.0).

2.5. Molecular docking

The prepared proteins were then submitted to the grid-generation protocol using two strategies for binding pocket detection. In the first strategy, grids were generated using a molecular probe available on OEDocking suite v.3.2.0.2 (OEDocking, n.d.; McGann, 2011, 2012) for detection of binding pockets around the protein. In the second strategy, co-crystallized ligands were considered geometric centers of the grids. Grid details are available in Supplementary Table S1. Finally, molecular docking calculations were performed using the high-resolution protocol of HYBRID program with the ChemGauss4 score function (McGann, 2011, 2012; McGann et al., 2003), available on OEDocking suite (OEDocking, n.d.; McGann, 2011, 2012).

3. Nonlinear optical property: Computational details

The electrical properties of the DFC crystal were studied using the supermolecule method (SM) to simulate the crystalline environment polarization on one DFC isolated molecule. This approach works with a bulk consisting of a set of $13 \times 13 \times 13$ unit cells. Each unit cell has 4 asymmetric units and each unit has 37 atoms, creating a bulk with 325,156 atoms. Fig. 1 show a schematic representation of one DFC isolated molecule

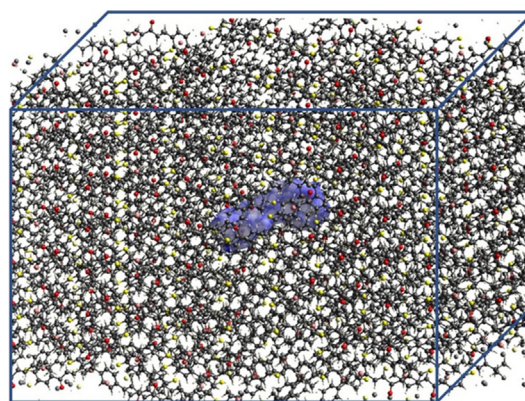


Fig. 1 An outline of the DFC bulk.

(highlighted in blue) inside the DFC bulk. The atoms that surrounded the isolated molecule were considered as point charges, and the molecular electrostatic potential was calculated via CHELPG with the MP2/6-311+G(d). The iterative process of the SM approach continues with the substitution of the partial atomic charges in each calculation step, until the convergence of the electric dipole moment is reached, see Fig. 2. Good results for the electric parameters of organic crystals were obtained with this calculation technique in comparison with experimental data (Castro et al., 2017, 2016; Valverde et al., 2018, 2017a, 2017b, 2012; Almeida et al., 2017; Vaz et al., 2016; Custodio et al., 2018; Baseia et al., 2017; Rodrigues et al., 2017, 2015). More recently, the third-order electric susceptibility of a chalcone derivative crystal calculated via the SM approach and the DFT/CAM-B3LYP/6-311+G(d) calculation model found good agreement with the Z-scan experimental data (Valverde et al., 2018).

The components and the average values of the electric parameters such as the electric dipole moment, (μ_i , $\langle \mu \rangle$), the linear polarizability (α_{ij} , $\langle \alpha \rangle$) and anisotropy of the linear polarizability ($\Delta\alpha$) were calculated using the MP2 theory. Density Functional Theory (DFT) at CAM-B3LYP level was employed for the calculation of the components and the average values of the second hyperpolarizability (γ_{ijkl} , $\langle \gamma \rangle$). The 6-311+G(d) basis set was used in both calculation methods.

The electrical parameters of the DFC embedded molecules were calculated using the following expressions,

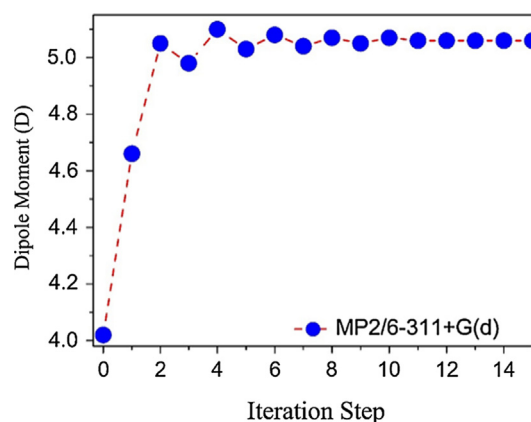


Fig. 2 MP2/6-311+G(d) dipole moment convergence.

$$\mu = \left(\mu_x^2 + \mu_y^2 + \mu_z^2 \right)^{\frac{1}{2}}, \quad (1)$$

$$\langle \alpha \rangle = \frac{\alpha_{xx} + \alpha_{yy} + \alpha_{zz}}{3}, \quad (2)$$

$$\Delta \alpha = 2^{-1/2} \left[(\alpha_{xx} - \alpha_{yy})^2 + (\alpha_{yy} - \alpha_{zz})^2 + (\alpha_{zz} - \alpha_{xx})^2 + 6(\alpha_{xz}^2 + \alpha_{xy}^2 + \alpha_{yz}^2) \right]^{1/2}, \quad (3)$$

$$\beta_{total} = \left[(\beta_{xxx} + \beta_{yyy} + \beta_{zzz})^2 + (\beta_{yyz} + \beta_{yzz} + \beta_{yxx})^2 + (\beta_{zzz} + \beta_{zxx} + \beta_{zyy})^2 \right]^{\frac{1}{2}}, \quad (4)$$

$$\langle \gamma \rangle = \frac{1}{15} \sum_{i,j=x,y,z} (\gamma_{ijj} + \gamma_{ijj} + \gamma_{ijj}). \quad (5)$$

Here, the medium optical dispersion was not taken into account; therefore, the mean value (or absolute value) of the static second hyperpolarizability can be simplified by using the Kleinman (1962) approximation and calculated by,

$$\langle \gamma \rangle = \frac{1}{5} [\gamma_{xxxx} + \gamma_{yyyy} + \gamma_{zzzz} + 2(\gamma_{xxyy} + \gamma_{xxzz} + \gamma_{yyzz})], \quad (6)$$

The average linear polarizability ($\langle \alpha \rangle$) can be related with the linear refractive index (n) of the crystal by the Clausius-Mossotti relationship, which is given by

$$\frac{n^2 - 1}{n^2 + 2} = \frac{4\pi N}{3} \langle \alpha \rangle, \quad (7)$$

where N is the number of molecules per unit cell volume. The third-order electric susceptibility ($\chi^{(3)}$) is related with the average second hyperpolarizability ($\langle \gamma \rangle$) by the expression,

$$\chi^{(3)} = f^4 N \langle \gamma \rangle, \quad (8)$$

where f is the Lorentz local field correction factor given by $f = (n^2 + 2)/3$. All the numerical results for the tensors polarizability and hyperpolarizability were obtained from the Gaussian 09 (Frisch et al., 2009) output file and converted by electronic units (*esu*).

4. Results and discussion

4.1. Solid state characterization

The compound crystallized into monoclinic centrosymmetric space group P21/n, with cell parameters $a = 8.4153(6)$ Å; $b = 5.8600(4)$ Å; $c = 29.727(2)$ Å; $\alpha = \gamma = 90^\circ$, $\beta = 95.656(2)^\circ$, $V = 1458.81(18)$ Å³, final indices $R_I = 0.0594$ and goodness-of-fit = 1.071. The crystallographic data for the final structural refinements are shown in Table 1, followed by the ellipsoid displacement plot of the asymmetric unit of DFC in Fig. 3. The angle between the planes of the aromatic rings A and B indicates non-planarity of the structure ($\chi = 53.36^\circ$). A syn-periplanar conformation is adopted by the carbonyl group in relation to the fluorinated aromatic ring, as confirmed by the dihedral angle C1–C6–C7=O1 ($\omega_1 = 24.33^\circ$).

The supramolecular arrangement of DFC is stabilized by four non-classical hydrogen bonds. A chain is observed, formed by two DFC molecules assembled in $R_2^1(7)$ ring motif through the bifurcated interaction C5–H5...O1...H8–C8

Table 1 Crystal data and refinement parameters used for DFC.

Formula weight	268.32 u.a
Temperature	296 (2) K
Wavelength	0.71073 Å
Crystal system	Monoclinic
Space group	P21/n
Unit cell dimensions	a = 8.4153(6) Å b = 5.8600(4) Å c = 29.727(2) Å $\beta = 95.656(2)^\circ$
Volume	1458.83 Å ³
Z, calculated density	4, 1.222 mg m ⁻³
Absorption coefficient	0.083 mm ⁻¹
F(000)	568
Reflections collected/unique	17,244/3006
Refinement method	Least square
Goodness-of-fit on F2	Least square
Goodness-of-fit on F2	1.065
Final R indexes [I > 2σ(I)]	0.0594

(Fig. 4a). Although weak, intermolecular interactions involving the fluorine atom stabilize the DFC crystal packing by forming two dimers. The first one, seen in Fig. 4b, involves the fluorine atom and an aromatic hydrogen in a $R_2^2(22)$ ring motif, while the other is composed of two DFC molecules assembled in a $R_2^2(22)$ ring motif by means of the fluorine atom and a methyl hydrogen (Fig. 4c). Geometric parameters of intermolecular interactions stabilizing the DFC crystal packing (Fig. 4d) are given in Table 2.

4.2. Target prediction

The potential biological targets for DFC were predicted using two different approaches. Initially, the DFC compound was fitted against thousands of structure-based pharmacophores using PharmMapper web server. (Liu et al., 2010; Wang et al., 2017) Subsequently, potentially interacting targets with the top 13 ranked Z'-scores were selected for further investigation (see Tables S1 and 3). The Z'-score is a better descriptor for ranked targets generated from the molecule's fit score and a library score matrix calculated beforehand. This score does not only apply to the pharmacophore matching but also considers a normal distribution that a randomly given molecule's fit score may follow.

After the target prioritization, molecular docking was used to investigate the binding affinity and intermolecular interactions for DFC at the binding sites of the predicted targets. As can be seen in Tables S1 and S3, docking scores demonstrate that DFCs have higher affinity to the enoyl-acyl carrier protein reductase (InhA) from *Mycobacterium tuberculosis* (Chem-Gauss4 score of -16.36). InhA is a key enzyme for the type II fatty acid synthesis (e.g. mycolic acids) of *M. tuberculosis*, which catalyzes NADH-dependent reduction of 2-trans-enoyl-acyl carrier protein to yield NAD⁺ and reduced enoyl thioester-ACP substrate (Marrakchi et al., 2000; AlMatar et al., 2018). Due to this excellent docking score, we suggest that DFC could be investigated as a potential antituberculosis agent.

Fig. 5 illustrates the predicted binding mode of DFC into the active site of InhA. The overall binding mode of DFC (Fig. 5a) is similar to the co-crystallized ligand *N*-(4-methylben

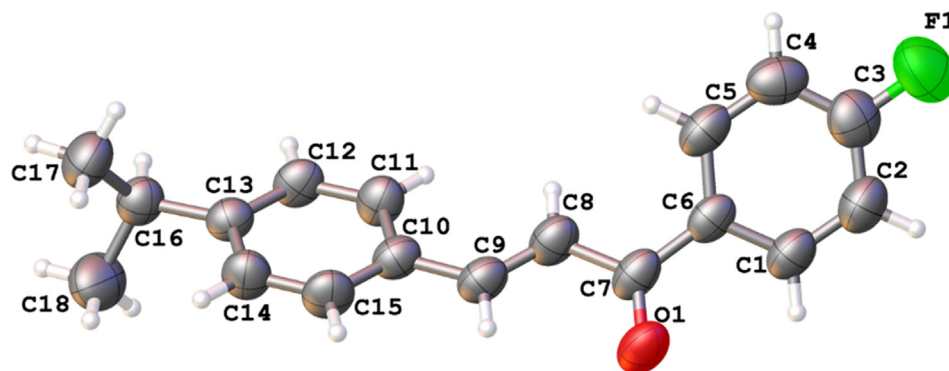


Fig. 3 ORTEP diagram of ellipsoids at the 50% probability level with the atomic numbering scheme for DFC. All bonds are in the normal range, and hydrogen atoms are shown as spheres of arbitrary radii.

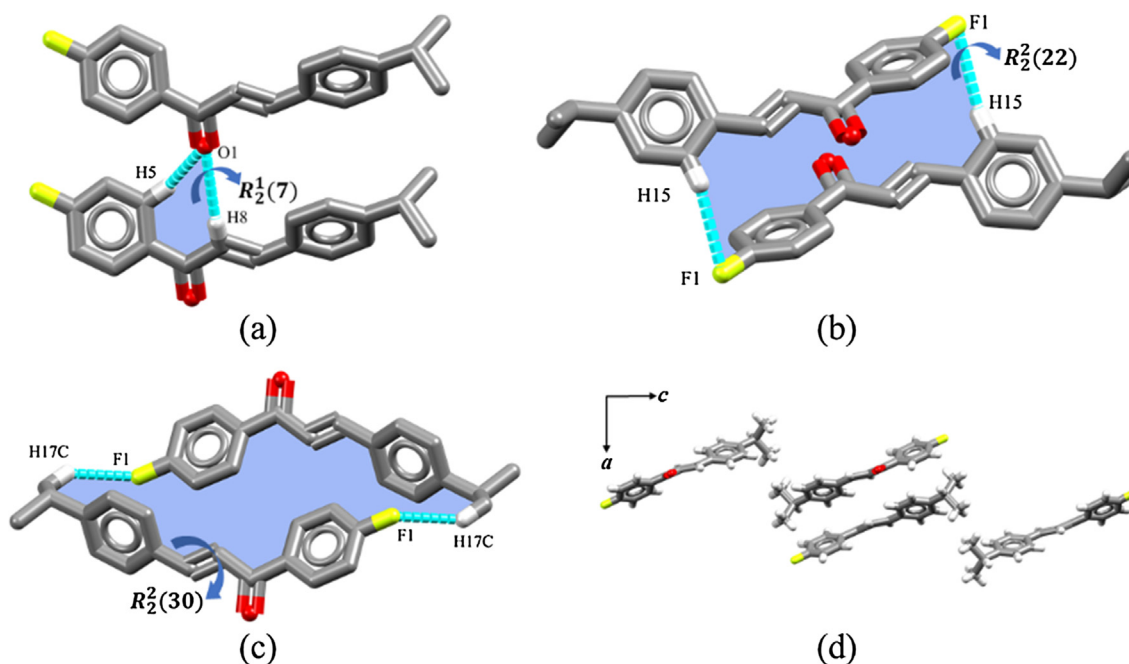


Fig. 4 Intermolecular interactions of DFC in (a), (b), (c) and its crystal packing (d).

Table 2 Intermolecular interactions observed for DFC.

D—H...A (Å)	D—H (Å)	H—A (Å)	D—A (Å)	D—H...A (°)
C15—H15...F1 ⁽ⁱ⁾	0.930	2.859	3.713	153.35
C17—H17C...F1 ⁽ⁱⁱ⁾	0.960	2.741	3.567	144.64
C8—H8...O1 ⁽ⁱⁱⁱ⁾	0.930	2.852	3.754	163.61
C5—H5...O1 ⁽ⁱⁱⁱ⁾	0.930	2.861	3.608	139.52

(i) = 1-x,-y,-z; (ii) = 1-x, 1-y,-z and (iii) = x,1 + y,z.

zoyl)-4-benzylpiperidine in the crystal structure (Fig. 5b) (He et al., 2007). The carbonyl of DFC forms two hydrogen-bond interactions with the 2'-hydroxyl group of NAD (co-factor highlighted in orange), and hydroxyl of Tyr158. In addition, the 4-isopropylphenyl moiety forms a π -stacking interaction with Phe149 and van der Waals interactions with residues Leu218, Trp222, Pro193, Ile215, and Val203. Moreover, structural analysis shows that the predicted binding mode of DFC

with InhA allows for several van der Waals interactions is found between the 4-fluorophenyl moiety of the DFC and Met103, Met161, Ala198, and Ile202.

4.3. DFC optical properties

Table 4 shows the MP2/6-311+G(d) results for the total dipole moment (and its components) for both the isolated

Table 3 Top five predicted targets.

Protein target (organism)	Fit Score	Z'-score	Docking score
InhA (<i>M. tuberculosis</i>)	3.70	3.78	-16.36
Aldose reductase (Homo sapiens)	3.58	3.52	-13.87
Poly (ADP-ribose polymerase 1 (Homo sapiens)	3.42	2.63	-10.47
Palmitoyl-proteinthioesterase 1 (Bostaurus)	3.55	2.60	-10.33
β -lactamase TEM (<i>Escherichia coli</i>)	3.51	2.82	-9.36

and embedded DFC molecules. As can be seen, the effects of the crystalline environment polarization cause an enhancement of the total dipole moment of 25.9%, from 4.02D to 5.06D. The absolute value of the μ_x decreases, while components μ_y and μ_z are enhanced by 38.9% and 10.4% respectively. However, the average linear polarizability is practically insensitive to the environment's polarization effects, as can be seen in Table 4, and the α_{ij} -values present a percentage variation smaller than 3.2%.

The DFT/CAM-B3LYP/6-311+G(d) results for the second hyperpolarizability $\langle\gamma\rangle$ and γ_{ijkl} are shown in Table 5. As can be observed, the environment's polarization effects on the $\langle\gamma\rangle$ -value present an increase of 6.1%, and on the second hyperpolarizability components (γ_{ijkl}) the percentage deviation stands between 2.3% and 7.1%.

4.3.1. Dynamic results

The nonlinear refractive index of the DFC crystal was determined from Eq. (7) of $n = 1.629$ and the third-order electric susceptibility ($\chi^{(3)}$), was done through Eq. (8), using the value of the average second hyperpolarizability of 66.92×10^{-36} esu and the value found was of $\chi^{(3)} = 14,800$ (pm/V)² in the static case, when comparing third-order electrical susceptibility with experimental values of chalcone derivatives measured by the z-scan technique of the crystals 4Br4MSP, 3Br4MSP, 4N4MSP, and CTDMP respectively (Rodrigues et al., 2017), the value for DFC is 64.50, 74.55, 62.60, and 6.23 times higher than

Table 4 MP2/6-311+G(d) results for the dipole moment (D) and linear polarizability (10^{-24} esu) for DFC isolated and embedded molecules.

	Isolated	Embedded		Isolated	Embedded
μ_x	-1.28	-1.19	α_{xx}	23.85	23.96
μ_y	3.03	4.21	α_{xy}	-1.90	-1.96
μ_z	2.30	2.54	α_{yy}	26.86	27.00
μ	4.02	5.06	α_{xz}	-10.89	-11.13
			α_{yz}	5.01	5.11
			α_{zz}	41.60	41.84
			$\langle\alpha\rangle$	30.77	30.94

those values, respectively. The typical value of $\chi^{(3)}$ reported in the literature is of the order of $100(\text{pm/V})^2$ (Rodrigues et al., 2015).

The DFT/CAM-B3LYP/6-311+G(d) results for the dc-Second Harmonic Generation function, $\langle\gamma(-2\omega; \omega, \omega, 0)\rangle$, as a function of the electric field frequency, are shown in Fig. 6c and d. As one can see, this function presents a monotonic increase in the region $\omega \leq 0.072$ a.u. (Fig. 6c), where the $\langle\gamma(-2\omega; \omega, \omega, 0)\rangle$ -values increase from 63.1 to 865.2 (in units of 10^{-36} esu) for the isolated molecule and from 66.9 to 1138.64 (in units of 10^{-36} esu) for the embedded molecule, presenting a factor of increase of 13.7 and 17.0 times the static values respectively. Clearly, a well-defined sharp peak can be observed at the resonant frequency in the vicinity of $\omega = 0.08$ a.u. (Fig. 6d).

4.3.2. Third-order nonlinear susceptibility

From Eq. (7), the linear refractive index value of the DFC crystal was determined as $n = 1.629$. From Eq. (8), the third-order electric susceptibility ($\chi^{(3)}$) was estimated using the value of the average second hyperpolarizability of 66.92×10^{-36} esu, and the value found was of $\chi^{(3)} = 14,800$ (pm/V)² in the static case. This is compared to the third-order electrical susceptibility with experimental values of chalcone derivatives measured by the Z-scan technique for the crystals 4Br4MSP, 3Br4MSP, 4N4MSP, and CTDMP respec-

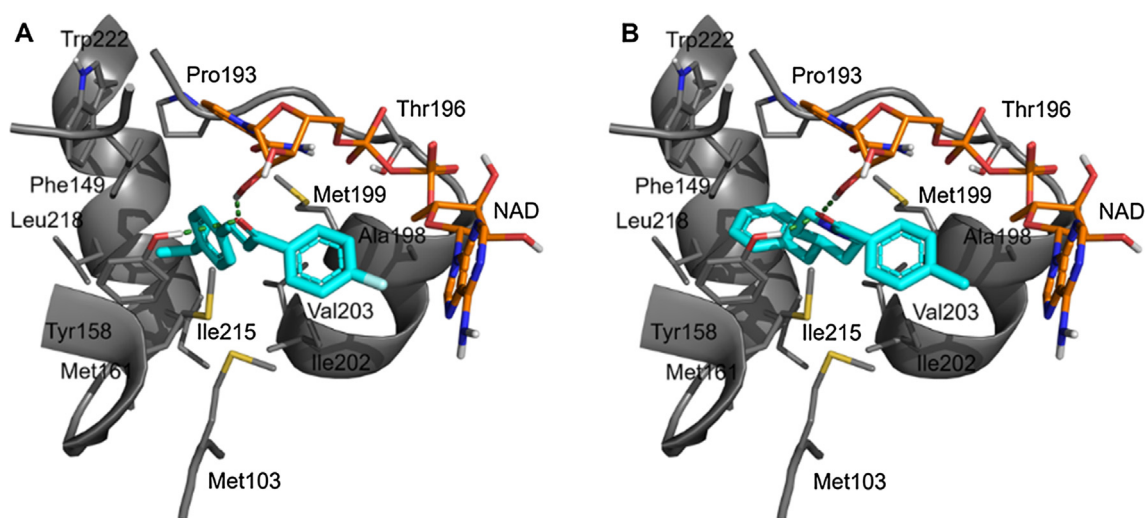
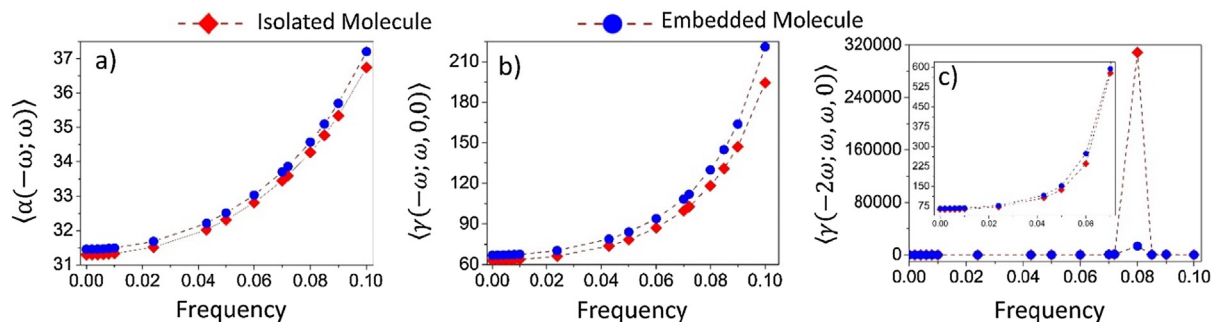
**Fig. 5** Intermolecular interactions of DFC (A) and co-crystallized ligand (B) at the active site of InhA from *Mycobacterium tuberculosis*.

Table 5 DFT/CAM – B3LYP results for the DFC average second hyperpolarizability (10^{-36} esu).

	γ_{xxxx}	γ_{yyyy}	γ_{zzzz}	γ_{xxyy}	γ_{yyzz}	γ_{xxzz}	$\langle \gamma \rangle$
Isolated	23.34	16.24	123.82	10.46	28.30	37.28	63.10
Embedded	23.89	16.95	132.64	11.04	29.97	39.53	66.92

**Fig. 6** Dynamic average linear polarizability $\langle \alpha(-\omega; \omega) \rangle$ and the average hyperpolarizabilities $\langle \gamma(-\omega; \omega, 0, 0) \rangle$ and $\langle \gamma(-2\omega; \omega, \omega, 0) \rangle$ as function of the electric field frequency for the isolated and embedded DFC molecules.

tively (D'silva et al., 2012), and using the equations the value for DFC is 64.50, 74.55, 62.60, and 6.23 times higher than those values, respectively. The typical value of $\chi^{(3)}$ reported in the literature is in the order of $100(\text{pm}/\text{V})^2$ (Günter, 2000).

4.3.3. Solvent results

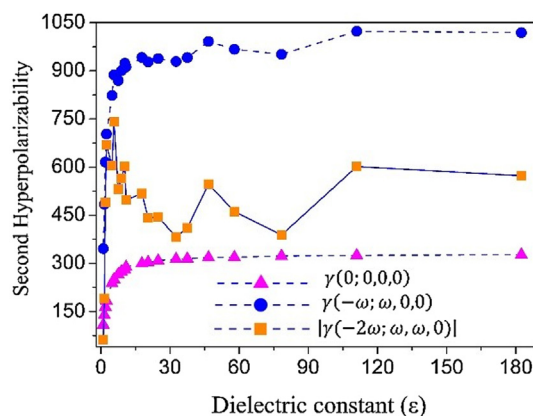
The effects of various solvent media on the static and dynamic electric properties of the DFC isolated molecule are shown in Tables S2 and S3. It is well known that when immersed in a solvent medium the electrical parameters of organic compounds present important changes, and therefore the following solvent media were considered: gas-phase ($\epsilon = 1.00$), argon ($\epsilon = 1.5$), heptane ($\epsilon = 1.9$), toluene ($\epsilon = 2.38$), chloroform ($\epsilon = 4.81$), chlorobenzene ($\epsilon = 5.69$); tetrahydroFuran ($\epsilon = 7.52$); dichloromethane ($\epsilon = 8.93$); dichloroethane ($\epsilon = 10.36$); 2-methyl-2-propanol ($\epsilon = 10.9$); 1-butanol ($\epsilon = 17.8$); acetone ($\epsilon = 20.49$); ethanol ($\epsilon = 24.85$); methanol ($\epsilon = 32.61$); acetonitrile ($\epsilon = 37.5$); dimethyl sulfoxide ($\epsilon = 46.70$); formic acid ($\epsilon = 57.9$); water ($\epsilon = 78.36$); formamide ($\epsilon = 111$) and n-methylformamide- mixture ($\epsilon = 182.4$), where ϵ is the static dielectric constant of the medium.

In Table S2 the CAM-B3LYP/6-311 + G(d) static results for the total electric dipole, the average linear polarizability, the z-component of first hyperpolarizability and the average second hyperpolarizability for the isolated DFC molecule in solvent media are presented. The results for the gas-phase are also shown for comparison. Note that the values of all the electrical parameters increase (in absolute value) with the increase in the solvent medium static dielectric constant. From the Argone ($\epsilon = 1.5$) to n-methylformamide-mixture ($\epsilon = 182.4$), the values of the electric parameters μ , $\langle \alpha(0, 0, 0) \rangle$, $\beta_{||z}(0, 0, 0)$ and $\langle \gamma(0; 0, 0, 0) \rangle$ show a percentage increase of 28.2%, 27.9%, 127.4% and 135.3%, respectively. The increase of these parameters with the increase of the dielectric constant value is not linear, as can be seen in Fig. 7, where the static and dynamics average second hyperpolarizability were plotted as a function of the dielectric constant values. As can be seen, the curve presents a saturation for larger dielectric constant values.

In Table S3 we present our results for $\alpha(-\omega; \omega)$, $\beta_{||z}(-\omega; \omega, 0)$, $\beta_{||z}(-2\omega; \omega, \omega)$, $\gamma(-\omega; \omega, 0, 0)$ and $\gamma(-2\omega; \omega, \omega, 0)$ for $\omega = 0.085\text{a.u.}$ in several solvent media. At this frequency the values of the linear polarizability are all positive and present an increase of 11% from argon to formamide, which is the solvent medium where $\alpha(-\omega; \omega)$ gives rise to the highest value (51.08×10^{-24} esu). The first hyperpolarizabilities shown in Table S3 present a different signal, and it is noted that the values of $\beta_{||z}(-\omega; \omega, 0)$ are all negative, while the values of $\beta_{||z}(-2\omega; \omega, \omega)$ are all positive. In contrast, the values of the second hyperpolarizabilities, $\gamma(-\omega; \omega, 0, 0)$ and $\gamma(-2\omega; \omega, \omega, 0)$, are positive and negative respectively, as shown in Table S3.

The average value of the Hyper Rayleigh Scattering first hyperpolarizability (β_{HRS}) can be calculated by the following expression and described in Bersohn et al. (1966) and Verbiest et al. (2009):

$$\langle \beta_{HRS} \rangle = \sqrt{\langle \beta_{ZZZ}^2 \rangle + \langle \beta_{XZZ}^2 \rangle} \quad (9)$$

**Fig. 7** Variation of the second hyperpolarizability as function of the dielectric constant of the solvent media.

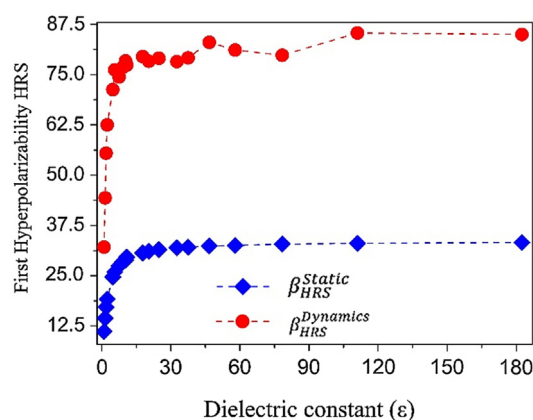


Fig. 8 Variation of the first hyperpolarizability (in 10^{-30} esu) as a function of the dielectric constant of the solvent medium dielectric constant values.

in which $\langle \beta_{zzz}^2 \rangle$ and $\langle \beta_{xzz}^2 \rangle$ are macroscopic averages. The results of the quantum-chemical calculations for the static ($\beta_{HRS}(0;0,0)$) and dynamic ($\beta_{HRS}(-\omega; \omega, \omega)$) first molecular hyperpolarizabilities of the DFC molecule in gas-phase and in several solvent media are displayed in Fig. 8. As can be seen, the β_{HRS} static and dynamic ($\omega = 0.0428 a.u.$) values present an increase following an increase in the ϵ -value.

5. Conclusions

DFC compound was crystallized in the $P2_1/n$ centrosymmetric space group. The molecules are connected by means of C—H...O and C—H...F intermolecular contacts, forming dimers which play an important role in the stabilization of crystal packing. The molecular modeling studies indicated that this compound could act as an anti-tuberculosis hit candidate, because of its high binding affinity with *M. tuberculosis* InhA. Also, theoretical calculations using the MP2/6-311+G(d) and the DFT/CAM-B3LYP/6-311+G(d) were performed to evaluate the NLO properties of DFC isolated and embedded molecules. From the obtained values of the average linear polarizability and of the average second hyperpolarizability, the linear refractive index and the nonlinear third-order susceptibility for DFC crystal were determined. The static value $\chi^{(3)} = 14,800$ (pm/V)² is several magnitude orders greater than the $\chi^{(3)}$ -values reported for other chalcone derivatives, indicating that the DFC crystal has good potential for study as a NLO material. The effects of several solvent media on the DFC electrical parameter (isolated molecule) complete our studies of the NLO properties of DFC. In addition, this work enabled a better understanding of the structural properties of fluoride chalcones, as well as structural and supramolecular characteristics.

Acknowledgements

The authors gratefully acknowledge the financial support of the Conselho Nacional de Desenvolvimento Científico e Tecnológico (CNPq), Coordenação de Aperfeiçoamento de Pessoal de Nível Superior (CAPES) and Fundação de Amparo a Pesquisa do Estado de Goiás (FAPEG). We are also grateful

to ChemAxon and OpenEye Inc., for providing us with academic licenses of their software.

Appendix A. Supplementary material

Supplementary data to this article can be found online at <https://doi.org/10.1016/j.arabjc.2018.11.010>.

References

- Abu, N., Ho, W., Yeap, S., Akhtar, M., Abdullah, M., Omar, A., Alitheen, N., 2013. The flavokawains: uprising medicinal chalcones. *Cancer Cell Int.* 13, 102. <https://doi.org/10.1186/1475-2867-13-102>.
- Allen, F.H., 2002. The Cambridge Structural Database: a quarter of a million crystal structures and rising. *Acta Crystallogr. Sect. B Struct. Sci.* 58, 380–388. <https://doi.org/10.1107/S0108768102003890>.
- AlMatar, M., Makky, E.A., Var, I., Kayar, B., Köksal, F., 2018. Novel compounds targeting InhA for TB therapy. *Pharmacol. Rep.* 70, 217–226. <https://doi.org/10.1016/j.pharep.2017.09.001>.
- Almeida, L.R., Anjos, M.M., Ribeiro, G.C., Valverde, C., Machado, D.F.S., Oliveira, G.R., Napolitano, H.B., de Oliveira, H.C.B., 2017. Synthesis, structural characterization and computational study of a novel amino chalcone: a potential nonlinear optical material. *New J. Chem.* 41, 1744–1754. <https://doi.org/10.1039/C5NJ03214H>.
- Anandakrishnan, R., Aguilar, B., Onufriev, A.V., 2012. H++ 3.0: automating pK prediction and the preparation of biomolecular structures for atomistic molecular modeling and simulations. *Nucl. Acids Res.* 40, W537–W541. <https://doi.org/10.1093/nar/gks375>.
- Baseia, B., Osório, F., Lima, L., Valverde, C., 2017. Effects of changing substituents on the non-linear optical properties of two coumarin derivatives. *Crystals* 7, 158. <https://doi.org/10.3390/cryst7060158>.
- Battle, G.M., Ferrence, G.M., Allen, F.H., 2010. Applications of the Cambridge Structural Database in chemical education. *J. Appl. Crystallogr.* 43, 1208–1223. <https://doi.org/10.1107/S0021889810024155>.
- Bersohn, R., Yoh-Han, P.A.O., Frisch, H.L., 1966. Double-quantum light scattering by molecules. *J. Chem. Phys.* 45, 3184–3198. <https://doi.org/10.1063/1.1728092>.
- Calloway, N.O., Green, L.D., 1937. Reactions in the presence of metallic halides. I. β -unsaturated ketone formation as a side reaction in friedel–crafts acylations. *J. Am. Chem. Soc.* 59, 809–811. <https://doi.org/10.1021/ja01284a011>.
- Carvalho, P.S., Custodio, J.M.F., Vaz, W.F., Cirilo, C.C., Cidade, A. F., Aquino, G.L.B., Campos, D.M.B., Cravo, P., Coelho, C.J., Oliveira, S.S., Camargo, A.J., Napolitano, H.B., 2017. Conformation analysis of a novel fluorinated chalcone. *J. Mol. Model.* 23. <https://doi.org/10.1007/s00894-017-3245-8>.
- Castro, A.N., Almeida, L.R., Anjos, M.M., Oliveira, G.R., Napolitano, H.B., Valverde, C., Baseia, B., 2016. Theoretical study on the third-order nonlinear optical properties and structural characterization of 3-Acetyl-6-Bromocoumarin. *Chem. Phys. Lett.* 653, 122–130. <https://doi.org/10.1016/j.cplett.2016.04.070>.
- Castro, A.N., Osório, F.A.P., Ternavisk, R.R., Napolitano, H.B., Valverde, C., Baseia, B., 2017. Theoretical investigations of nonlinear optical properties of two crystalline acetamides structures including polarization effects of their environment. *Chem. Phys. Lett.* 681, 110–123. <https://doi.org/10.1016/j.cplett.2017.05.066>.
- Climont, M.J., Corma, A., Iborra, S., Primo, J., 1995. Base catalysis for fine chemical production: Claisen-Schmidt condensation on zeolites and hydrotalcites for the production of chalcones and flavanones of pharmaceutical interest. *J. Catal.* 151, 60–66.

- Custodio, J.M.F., Santos, F.G., Vaz, W.F., Cunha, C.E.P., Silveira, R. G., Anjos, M.M., Campos, C.E.M., Oliveira, G.R., Martins, F.T., da Silva, C.C., Valverde, C., Baseia, B., Napolitano, H.B., 2018. Molecular structure of hybrid imino-chalcone in the solid state: X-ray diffraction, spectroscopy study and third-order nonlinear optical properties. *J. Mol. Struct.* 1157. <https://doi.org/10.1016/j.molstruc.2017.12.023>.
- D'silva, E.D., Podagatlapalli, G.K., Venugopal Rao, S., Dharmaprakash, S.M., 2012. Study on third-order nonlinear optical properties of 4-methylsulfanyl chalcone derivatives using picosecond pulses. *Mater. Res. Bull.* 47, 3552–3557. <https://doi.org/10.1016/j.materresbull.2012.06.063>.
- Das, A., Krishna Reddy, A.G., Krishna, J., Satyanarayana, G., 2014. An efficient synthesis of highly substituted indanones and chalcones promoted by superacid. *RSC Adv.* 4, 26662–26666. <https://doi.org/10.1039/C4RA04763J>.
- Díaz-Tielas, C., Graña, E., Reigosa, M.J., Sánchez-Moreiras, A.M., 2016. Biological activities and novel applications of chalcones. *Planta Daninha* 34, 607–616. <https://doi.org/10.1590/S0100-83582016340300022>.
- Farrugia, L.J., 2012. WinGX and ORTEP for Windows: an update. *J. Appl. Crystallogr.* 45, 849–854. <https://doi.org/10.1107/S0021889812029111>.
- Ferreira, J.V.R., Peckle, B.A., da Silva, A.S., Gomes, A.daS., Santana, V.M., Direito, I.C.N., 2014. Pesticidas aplicados na lavoura e o risco à saúde pública: uma revisão da literatura, *Cad. UniFOA*, pp. 85–94.
- Frisch, M.J., Trucks, G.W., Schlegel, H.B., Scuseria, G.E., Robb, M. A., Cheeseman, J.R., Scalmani, G., Barone, V., Mennucci, B., Petersson, G.A., Nakatsuji, H., Caricato, M., Li, X., Hratchian, H. P., Izmaylov, A.F., Bloino, J., Zheng, G., Sonnenberg, J.L., Hada, M., Ehara, M., Toyota, K., Fukuda, R., Hasegawa, J., Ishida, M., Nakajima, T., Honda, Y., Kitao, O., Nakai, H., Vreven, T., Montgomery Jr., J.A., Peralta, J.E., Ogliaro, F., Bearpark, M., Heyd, J.J., Brothers, E., Kudin, K.N., Staroverov, V.N., Kobayashi, R., Normand, J., Raghavachari, K., Rendell, A., Burant, J.C., Iyengar, S.S., Tomasi, J., Cossi, M., Rega, N., Millam, J.M., Klene, M., Knox, J.E., Cross, J.B., Bakken, V., Adamo, C., Jaramillo, J., Gomperts, R., Stratmann, R.E., Yazyev, O., Austin, A.J., Cammi, R., Pomelli, C., Ochterski, J.W., Martin, R.L., Morokuma, K., Zakrzewski, V.G., Voth, G.A., Salvador, P., Dannenberg, J.J., Dapprich, S., Daniels, A.D., Farkas, Ö., Foresman, J.B., Ortiz, J. V., Cioslowski, J., Fox, D.J., 2009. In: *Gaussian 09, Revision A.02*, vol. 4. Gaussian Inc Wallingford CT, Wallingford CT <http://doi.org/10.1159/000348293>.
- Gharib, A., Pesyan, N.N., Jahangir, M., Roshani, M., Scheeren, J.H. W., Bakhtiar, L., Mohadeszadeh, S., Lagzian, S., Ahmadi, S., 2014. Heteropolyacids accelerated multi-component synthesis of N-phenylquinazolin-4-Amines by using silica-supported Preyessler nanoparticles in green solvent. *Bulg. Chem. Commun.* 46, 215–222.
- Gomes, M.N., Braga, R.C., Grzelak, E.M., Neves, B.J., Muratov, E., Ma, R., Klein, L.L., Cho, S., Oliveira, G.R., Franzblau, S.G., Andrade, C.H., 2017. QSAR-driven design, synthesis and discovery of potent chalcone derivatives with antitubercular activity. *Eur. J. Med. Chem.* 137, 126–138. <https://doi.org/10.1016/j.ejmech.2017.05.026>.
- Gonçalves, L.M., Valente, I.M., Rodrigues, J.A., 2014. An overview on cardamonin. *J. Med. Food.* 17, 633–640. <https://doi.org/10.1089/jmf.2013.0061>.
- Gordon, J.C., Myers, J.B., Folta, T., Shoja, V., Heath, L.S., Onufriev, A., 2005. H++: a server for estimating pKas and adding missing hydrogens to macromolecules. *Nucl. Acids Res.* 33, W368–W371. <https://doi.org/10.1093/nar/gki464>.
- Günter, P., 2000. *Nonlinear Optical Effects and Materials*. Springer, Berlin Heidelberg <http://doi.org/10.1007/978-3-540-49713-4>.
- Hameed, A., Abdullah, M.I., Ahmed, E., Sharif, A., Irfan, A., Masood, S., 2016. Anti-HIV cytotoxicity enzyme inhibition and molecular docking studies of quinoline based chalcones as potential non-nucleoside reverse transcriptase inhibitors (NNRT). *Bioorg. Chem.* 65, 175–182. <https://doi.org/10.1016/j.bioorg.2016.02.008>.
- Hawkins, P.C.D., Skillman, A.G., Warren, G.L., Ellingson, B.A., Stahl, M.T., 2010. Conformer generation with OMEGA: algorithm and validation using high quality structures from the protein databank and Cambridge structural database. *J. Chem. Inf. Model.* 50, 572–584. <https://doi.org/10.1021/ci100031x>.
- He, X., Alian, A., Ortiz de Montellano, P.R., 2007. Inhibition of the Mycobacterium tuberculosis enoyl acyl carrier protein reductase InhA by arylamides. *Bioorg. Med. Chem.* 15, 6649–6658. <https://doi.org/10.1016/j.bmc.2007.08.013>.
- Jakalian, A., Jack, D.B., Bayly, C.I., 2002. Fast efficient generation of high-quality atomic charges. AM1-BCC model: II. Parameterization and validation. *J. Comput. Chem.* 23, 1623–1641. <https://doi.org/10.1002/jcc.10128>.
- Jioui, I., Dânon, K., Solhy, A., Jouiad, M., Zahouily, M., Essaid, B., Len, C., Fihri, A., 2016. Modified fluorapatite as highly efficient catalyst for the synthesis of chalcones via Claisen-Schmidt condensation reaction. *J. Ind. Eng. Chem.* 39, 218–225. <https://doi.org/10.1016/j.jiec.2016.06.003>.
- Kleinman, D.A., 1962. Nonlinear dielectric polarization in optical media. *Phys. Rev.* 126, 1977–1979. <https://doi.org/10.1103/PhysRev.126.1977>.
- Krawczyk, P., Pietrzak, M., Janek, T., Jędrzejewska, B., Cysewski, P., 2016. Spectroscopic and nonlinear optical properties of new chalcone fluorescent probes for bioimaging applications: a theoretical and experimental study. *J. Mol. Model.* 22, 125. <https://doi.org/10.1007/s00894-016-2990-4>.
- Liu, X., Ouyang, S., Yu, B., Liu, Y., Huang, K., Gong, J., Zheng, S., Li, Z., Li, H., Jiang, H., 2010. PharmMapper server: a web server for potential drug target identification using pharmacophore mapping approach. *Nucl. Acids Res.* 38, W609–W614. <https://doi.org/10.1093/nar/gkq300>.
- Macrae, C.F., Edgington, P.R., McCabe, P., Pidcock, E., Shields, G. P., Taylor, R., Towler, M., van de Streek, J., 2006. Mercury: visualization and analysis of crystal structures. *J. Appl. Crystallogr.* 39, 453–457. <https://doi.org/10.1107/S002188980600731X>.
- Mahapatra, D.K., Asati, V., Bharti, S.K., 2015. Chalcones and their therapeutic targets for the management of diabetes: structural and pharmacological perspectives. *Eur. J. Med. Chem.* 92, 839–865. <https://doi.org/10.1016/j.ejmech.2015.01.051>.
- Marrakchi, H., Lanéelle, G., Quémard, A., 2000. InhA, a target of the antituberculous drug isoniazid, is involved in a mycobacterial fatty acid elongation system, FAS-II. *Microbiology* 146, 289–296. <https://doi.org/10.1099/00221287-146-2-289>.
- Matos, M.J., Vazquez-Rodriguez, S., Uriarte, E., Santana, L., 2015. Potential pharmacological uses of chalcones: a patent review (from June 2011–2014). *Expert Opin. Ther. Pat.* 25, 351–366. <https://doi.org/10.1517/13543776.2014.995627>.
- McGann, M., 2011. FRED pose prediction and virtual screening accuracy. *J. Chem. Inf. Model.* 51, 578–596. <https://doi.org/10.1021/ci100436p>.
- McGann, M., 2012. FRED and HYBRID docking performance on standardized datasets. *J. Comput. Aided. Mol. Des.* 26, 897–906. <https://doi.org/10.1007/s10822-012-9584-8>.
- McGann, M.R., Almond, H.R., Nicholls, A., Grant, J.A., Brown, F.K., 2003. Gaussian docking functions. *Biopolymers* 68, 76–90.
- Murugesan, A., Gengan, R.M., Krishnan, A., 2017. Sulfonic acid functionalized boron nitride nano materials as a microwave-assisted efficient and highly biologically active one-pot synthesis of piperazinyl-quinolinyl fused Benzo[c]acridine derivatives. *Mater. Chem. Phys.* 188, 154–167. <https://doi.org/10.1016/j.matchemphys.2016.12.039>.
- Nardelli, M., nardelli1995.pdf, *J. Appl. Crystall.*, Parma, Italy, 1995. <https://doi.org/10.1107/S0021889895007138>.

- Nowakowska, Z., 2007. A review of anti-infective and anti-inflammatory chalcones. *Eur. J. Med. Chem.* 42, 125–137. <https://doi.org/10.1016/j.ejmech.2006.09.019>.
- OEDocking v.3.2.0, n.d., OpenEye Scientific Software, Santa Fe, NM. <http://www.eyesopen.com>.
- OMEGA 3.0.0.1: OpenEye Scientific Software, Santa Fe, NM. <http://www.eyesopen.com>. Hawkins, P.C.D.; Skillman, A.G.; Warren, G. L.; Ellingson, B.A.; Stahl, M.T., 2018.
- QUACPAC v.1.6.3, n.d., OpenEye Scientific Software, Santa Fe, NM. <http://www.eyesopen.com>.
- Rodrigues, R.F.N., Valverde, C., Baseia, B., de Oliveira, H.C.B., 2015. Hiperpolarizabilidade da L-arginina Fosfatada Monohidratada Considerando o Efeito do Ambiente Cristalino. *Rev. Process. Químicos* 9, 213–215.
- Rodrigues, R.F.N., Almeida, L.R., dos Santos, F.G., Carvalho Jr, P. S., de Souza, W.C., Moreira, K.S., de Aquino, G.L.B., Valverde, C., Napolitano, H.B., Baseia, B., 2017. Solid state characterization and theoretical study of non-linear optical properties of a Fluoro-N-Acylhydrazide derivative. *PLoS One*. 12, e0175859. <https://doi.org/10.1371/journal.pone.0175859>.
- Rosa, G.P., Seca, A.M.L., Barreto, M. do C., Pinto, D.C.G.A., 2017. Chalcone: a valuable scaffold upgrading by green methods. *ACS Sustain. Chem. Eng.* 5, 7467–7480. <https://doi.org/10.1021/acssuschemeng.7b01687>.
- Sheldrick, G.M., 2015. Crystal structure refinement with SHELXL. *Acta Crystallogr. Sect. C Struct. Chem.* 71, 3–8. <https://doi.org/10.1107/S2053229614024218>.
- Spackman, M.A., Jayatilaka, D., 2009. Hirshfeld surface analysis, pp. 19–32 <https://doi.org/10.1039/b818330a>.
- Szczesna, D., Koprowski, M., Różycka-Sokołowska, E., Marciniak, B., Balczewski, P., 2017. Selective Horner-Wittig/Nazarov vs Knoevenagel/Nazarov reactions in the synthesis of biologically active 3-aryl-substituted 1-indanones. *Synlett* 28, 113–116. <https://doi.org/10.1055/s-0036-1588599>.
- Valverde, C., Avelar, A.T., Baseia, B., 2012. Quantum communication via controlled holes in the statistical distribution of excitations in a nanoresonator coupled to a Cooper pair box. *Chinese Phys. B* 21, 030308. <https://doi.org/10.1088/1674-1056/21/3/030308>.
- Valverde, C., Vaz, W.F., Custodio, J.M.F., Duarte, V.S., Carvalho-Jr, P.S., Figueredo, A.S., de Aquino, G.L.B., Baseia, B., Napolitano, H.B., 2017a. The solid state structure and environmental polarization effect of a novel asymmetric azine. *New J. Chem.* 41, 11361–11371. <https://doi.org/10.1039/C7NJ00618G>.
- Valverde, C., Rodrigues, R.F.N., Machado, D.F.S., Baseia, B., de Oliveira, H.C.B., 2017b. Effect of the crystalline environment on the third-order nonlinear optical properties of L-arginine phosphate monohydrate: a theoretical study. *J. Mol. Model.* 23, 122. <https://doi.org/10.1007/s00894-017-3274-3>.
- Valverde, C., Osório, F.A.P., Fonseca, T.L., Baseia, B., 2018. DFT study of third-order nonlinear susceptibility of a chalcone crystal. *Chem. Phys. Lett.* 706, 170–174 <https://doi.org/10.1016/j.cplett.2018.06.001>.
- Vaz, W., Custodio, J., Silveira, R., Castro, A., Campos, C., Anjos, M., Oliveira, G., Valverde, C., Baseia, B., Napolitano, H., 2016. Synthesis, characterization, and third-order nonlinear optical properties of a new neolignane analogue. *R. Soc. Chem.* 6.
- Vaz, W.F., Custodio, J.M.F., Silveira, R.G., Castro, A.N., Campos, C. E.M., Anjos, M.M., Oliveira, G.R., Valverde, C., Baseia, B., Napolitano, H.B., 2016. Synthesis, characterization, and third-order nonlinear optical properties of a new neolignane analogue. *RSC Adv.* 6, 79215–79227. <https://doi.org/10.1039/C6RA14961H>.
- Verbiest, T., Clays, K., Rodriguez, V., 2009. Second-Order Nonlinear Optical Characterization Techniques. An Introduction, <http://doi.org/10.1201/9781420070736>.
- Wan, Z., Hu, D., Li, P., Xie, D., Gan, X., 2015. Synthesis, antiviral bioactivity of novel 4-thioquinazoline derivatives containing chalcone moiety. *Molecules* 20, 11861–11874. <https://doi.org/10.3390/molecules200711861>.
- Wang, X., Shen, Y., Wang, S., Li, S., Zhang, W., Liu, X., Lai, L., Pei, J., Li, H., 2017. PharmMapper 2017 update: a web server for potential drug target identification with a comprehensive target pharmacophore database. *Nucl. Acids Res.* 45, W356–W360. <https://doi.org/10.1093/nar/gkx374>.
- Zhou, B., 2015. Diverse molecular targets for chalcones with varied bioactivities. *Med. Chem. (Los. Angeles)*. <https://doi.org/10.4172/2161-0444.1000291>.